Acta of Bioengineering and Biomechanics
Vol. 17, No. 2, 2015

Original paper
DOI: 10.5277/ ABB-00046-2014-02

A finite element model of the L4-L5-S1 human spine segment including the heterogeneity and anisotropy of the discs

HECTOR E. JARAMILLO[1, 2], LESSBY GÓMEZ[1, 3], JOSE J. GARCÍA[1]*

[1] Universidad del Valle, Cali-Colombia.
[2] Universidad Autonoma de Occidente, Cali-Colombia.
[3] Universidad Libre, Cali-Colombia.

With the aim to study disc degeneration and the risk of injury during occupational activities, a new finite element (FE) model of the L4-L5-S1 segment of the human spine was developed based on the anthropometry of a typical Colombian worker. Beginning with medical images, the programs CATIA and SOLIDWORKS were used to generate and assemble the vertebrae and create the soft structures of the segment. The software ABAQUS was used to run the analyses, which included a detailed model calibration using the experimental step-wise reduction data for the L4-L5 component, while the L5-S1 segment was calibrated in the intact condition. The range of motion curves, the intradiscal pressure and the lateral bulging under pure moments were considered for the calibration. As opposed to other FE models that include the L5-S1 disc, the model developed in this study considered the regional variations and anisotropy of the annulus as well as a realistic description of the nucleus geometry, which allowed an improved representation of experimental data during the validation process. Hence, the model can be used to analyze the stress and strain distributions in the L4-L5 and L5-S1 discs of workers performing activities such as lifting and carrying tasks.

Key words: *intervertebral disc, L4-L5-S1 segment, finite element model, human spine, hyperelastic model*

1. Introduction

Low back pain is a disorder frequently found in a high percentage of the world population. There is a high economic and social impact associated with this dysfunction, which is often caused by pathologies originated in the lumbar spine. In turn, these pathologies are usually produced by excessive deformation or degeneration of the soft structures located between each pair of vertebraes, known as intervertebral discs [4]. Many experimental and theoretical studies have been carried out to better understand the biomechanics of the lumbar spine in order to reduce the risk of disc injury or degeneration.

Compared to experimental testing, theoretical models using the Finite Element (FE) method are a relatively inexpensive and fast way to accomplish the mechanical analysis of the human spine. In addition, theoretical simulations allow investigating the behavior of the lumbar spine under conditions that cannot be reproduced in *in vitro* or *in vivo* experiments. Many models have been developed to analyze the mechanical behavior of the lumbar spine between the L1 and L5 vertebras, e.g. [2], [8], [24], [25]. However, only four models have included the intervertebral disc located between L5 and the sacrum [3], [7], [9], [11], [17]. It is in the L5-S1 disc where hernias and degeneration are frequently documented since it is known to support the highest load in the spine. Additionally, the geometry of the L5-S1 segment has important variations with respect to that of other spine segments.

The model by Bellinpi et al. [3] uses an orthotropic description for the annulus and does not ac-

* Corresponding author: Jose Jaime García, Universidad del Valle, Cali, Colombia. E-mail: josejgar@gmail.com
Received: March 5th, 2014
Accepted for publication: September 16th, 2014

count for material nonlinearities as the discs are represented asa linear elastic material. On the other hand, Guan et al. [11] consider material nonlinearities with a hyperelastic formulation but do not include the anisotropy caused by the reinforcing fibers of the annulus. It has been shown that both the anisotropy and material nonlinearities play an important role in the mechanics of the spine [29]. The model by Ezquerro et al. [7], [9] includes a linear elastic description for the nucleus and the annulus matrix, and takes into account anisotropy and material nonlinearities by using cables attached to the nodes of the mesh, which makes the orientation of the fibers to be mesh-dependent. A more recent model by Moramarco et al. [17] takes into account anisotropy and material nonlinearities with a Neo-Hookean formulation for the nucleus, the annulus matrix, and the reinforcing fibers.

These four models have provided a reasonable approximation of experimental data for the intact segments. However, these models describe each component of the disc, the nucleus and the annulus, as homogeneous materials and do not consider the variation of the fiber angle with position, which has been shown to be an important factor that modifies the mechanics of the spine [22]. Moreover, the models by Moramarco et al. [17] and Bellini et al. [3] represent the nucleus as a cylinder, which does not appear to be a realistic representation for this component.

A finite element model that can provide an accurate approximation of stress and strain fields in the disc is a useful tool that can be used to assess the risk of injury of workers performing activities, such as lifting and carrying weights. Hence, the aim of this study was to develop and calibrate an FE model of the lumbar L4-L5-S1 segment considering the anthropometry of a typical Colombian worker. The model was oriented to provide an accurate assessment of the mechanical parameters in the intervertebral discs, which are the structures of the spine that are more prone to suffer injury and degeneration. Thus, the model included the representation of regional variations of material properties in the discs as well as the change of fiber orientation with position and a realistic geometry for the nucleus. This model will allow performing the analyses of stress and strain distributions in the lumbar discs of Colombian workers that lift and transport bags as part of their daily activities, which may lead to a more objective determination of the risk of injury compared to evaluations based on the maximum magnitude of the load.

2. Materials and methods

2.1. Geometry reconstruction

A 22 year old male subject was chosen representing the anthropometric data of a mean Colombian worker according to the parameters established by the Social Security Agency of Colombia [23]. The procedure described by Jaramillo et al. [15] was followed to develop the geometry. Briefly, axial images of the vertebrae in planes separated by 0.5 mm were obtained with a Siemens Avanto (Siemens, Berlin, Germany) computer tomography unit of 1.4 Teslas. Image segmentation was accomplished with the program Simpleware (Simpleware Ltd., Exeter, UK) while the program Blender (Foundation Blender, Amsterdam, Netherlands) was used to optimize and smooth the surface. The solid representations of the three vertebras were next accomplished with the program CATIA v5R21 (Dassault Systèmes, Vélizy-Villacoublay, France).

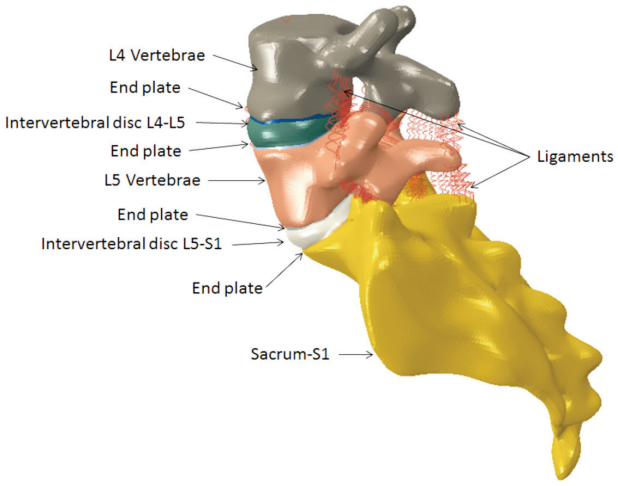

Fig. 1. Geometry of the finite element model

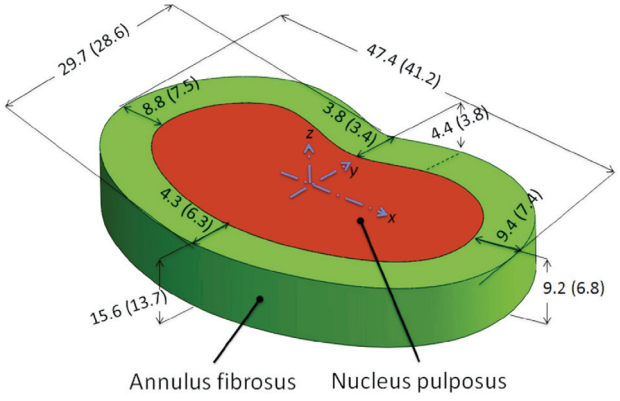

Fig. 2. Shape and dimensions in mm for the L4-L5 (first numbers) and L5-S1 (second numbers within parentheses) discs

These solid models were exported to the program SOLIDWORKS v2012 (Dassault Systèmes, Vélizy-Villacoublay, France) to assemble the three parts and create the soft structures, i.e., the intervertebral discs, the end plates and the articular cartilage of the facets. During this procedure, fluoroscopy images of the subject were used as a reference to locate the three vertebras and create the soft structures. Finally, this assembly was exported to the program ABAQUS v16.10-1 (Dassault Systèmes, Vélizy-Villacoublay, France) for the development of the finite element mesh and the inclusion of material properties, boundary conditions and loads (Fig. 1). Different to other finite element models [17], [24] that represent the nucleus of the intervertebral disc with a circular transverse section, the curve describing the external boundary of the nucleus followed the form of the external boundary of the disc (Fig. 2). For both discs, the percentage area of the nucleus with respect to the whole disc was near 50%. A convergence study was carried out taking as a reference the model developed by Ayturk et al. [2]. The final mesh of the disc contained eight division along the height and eight divisions along the radial directions of the annulus.

2.2. Constitutive equations

The main objective of the model was to analyze the stress and strain fields in the intervertebral discs. Hence, in order to improve the computational efficiency, the vertebrae were assumed to be rigid bodies. This simplification is supported by previous studies [16] showing that a model with rigid vertebrae predicts maximum stress values in the disc that are only 2% different with respect to those obtained with a model including the flexibility of the bone.

Consistent with other studies [2], [20], the annulus was represented as an isotropic hyperelastic matrix reinforced with two families of fibers. First, the following function W_m was used to describe the matrix

$$W_m = c_1(I_1 - 3) + c_2(I_1 - 3)^2 + c_3(I_1 - 3)^3 \qquad (1)$$

where c_1, c_2 and c_3 are material parameters and I_1 is the first deviatoric invariant of the Green deformation tensor. For the two families of reinforcing fibers, the following function W_f was utilized

$$W_f = \frac{a_1}{a_2[e^{a_2(I_4-1)^2} + e^{a_2(I_6-1)^2}]}, \qquad (2)$$

where a_1 and a_2 are material constants, and I_4 and I_6 are the deviatoric invariants associated with the two families of fibers, which are defined as

$$I_4 = N^{(1)}.C.N^{(1)}, \qquad (3)$$

$$I_6 = N^{(2)}.C.N^{(2)}, \qquad (4)$$

where $N^{(1)}$ and $N^{(2)}$ are the unit vectors along the two fiber directions in the non-deformed configuration, and C is the deviatoric right Green deformation tensor. The reinforcing fibers were assumed to be stressed only

Table 1. Summary of material properties and type of elements for the constituents of the model

Part name	Element type	Material model	Properties			Ref.
Annulus fibrosus	Hexahedral, 8 nodes, C3D8H	Hyperelastic, incompressible	Section	a_1 [MPa]	a_2 [Unitless]	[22]
			Anterior	1.20	14.40	
			Antero-lateral	0.85	10.20	
			Lateral	0.65	7.80	
			Postero-lateral	0.82	9.84	
			Posterior	0.85	10.20	
Bony endplates	Tetrahedral, 9 nodes, C3D10	Isotropic, linear elastic	E	1000 MPa		[2]
			ν	0.3		
L4, L5, Sacrum	Tetrahedral, 9 nodes, C3D10	Rigid body	Rigid body			[6]
Nucleus pulposus L4-L5, L5-Sacrum	Hexahedral, 8 nodes, C3D8	Hyperelastic, Neo-Hookean	c_{01}	0.06 MPa		[4]
			ν	0.49		
			D_1	0.16667 MPa		
			α	0.5 (1/°C)		
Ligaments	Non-linear spring, Spring A	Non-linear	Stress-strain curve			[18]

under a positive strain. A subroutine Uanisohyper of the program ABAQUS was developed to implement the aforementioned energy functions. Consistent with other studies [2], [22], the directions of the fibers varied with the radial coordinate from 25° on the outer boundary to 46° on the inner boundary, where this angle was measured with respect to the transverse plane.

Similar to Noailly et al. [18], the nucleus was described as a hyperelastic, Neo-Hookean material. The bony end plates were represented as a linear elastic material with an elasticity modulus E equal to 1000 MPa and a Poisson's ratio ν equal to 0.3 [4]. The ligaments were described as nonlinear springs [19] working only under tension. Material properties and type of elements are summarized in Table 1.

The annulus fibrosus of the L4-L5 and L5-S1 segments were divided into five sectors (Fig. 3) in order to take into account regional variations of material properties and to obtain a better adjustment of experimental data [22].

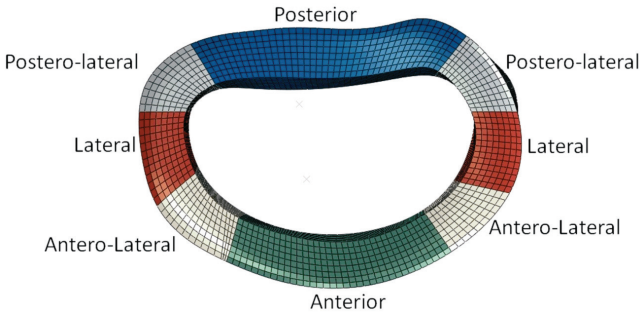

Fig. 3. Sections of the annulus fibrosus used to defined their different properties

2.3. Boundary conditions and prescribed rotations

In order to approximately represent the swelling caused by the osmotic pressure inside the nucleus, an initial step was included consisting of a change of temperature causing volumetric expansion, consistent with other models [2]. The validation process was accomplished in two phases as described below. During the first phase that was devoted to the L4-L5 segment, the caudal face of the L5 vertebra was assumed to be fixed while prescribed rotations were applied in the cranial surface of the L4 vertebra. In the second phase of the validation protocol for the intact L4-L5-S1, the sacral bone was assumed to be fixed while prescribed rotations were applied to the cranial surface of the L4 bone. The prescribed rotations were equal to 17°, which were applied along the three orthogonal axes. Results from these simulations with the whole L4-L5-S1 segment were processed to obtain the ROM curves for the L5-S1 unit that were needed to compare with the experimental data.

2.4. Model validation

To perform model calibration, the range of motion (ROM) curves under pure moments along the three orthogonal directions were considered [27]. It has been shown before [18] that there are many combinations of material parameters that can produce a reasonable fit of experimental ROM curves for the intact segment. Hence, in order to better assess the mechanical contribution of each component of the functional unit, the ROM curves obtained under the step-wise experimental protocol developed by Heuer et al. [13] for the L4-L5 segment were considered. Briefly, this experimental protocol consists of testing each functional unit several times, where a component of the unit is removed before each new test. After removing all of the ligaments and the posterior contacting surfaces, the final test is accomplished by removing the nucleus, leaving only the annulus between the two vertebrae.

Since the step-wise experimental reduction protocol has only been carried out for the L4-L5 unit, the first part of the model validation was performed with this segment, where the calibration proceeded in an order opposed to the experiments, i.e., the first phase began with the reduced L4-L5 unit containing only the annulus and the vertebral bodies, which allowed the determination of the annulus mechanical properties. Next, the calibration was successively repeated after adding the nucleus, the anterior longitudinal ligament, the posterior longitudinal ligament, the vertebral arches, the facet capsules, the flaval ligament, the interspinous ligament, the supraspinous ligament and finally the intertransversal ligaments.

The annulus was divided in anterior, posterior, lateral, antero-lateral, and postero-lateral regions in order to take into account the variation of properties with position and accomplish a better fitting of the experimental data (Fig. 3). The weighting factors $k_{ant} = 1.2$, $k_p = 0.85$, $k_l = 0.65$, $k_{al} = 0.85$, $k_{pl} = 0.82$, respectively, were applied to the stiffness of the anterior, posterior, lateral, antero-lateral and postero-lateral regions, consistent with Schmidt et al. [22].

After calibrating the L4-L5 unit as explained above, all the components of the L5-S1 unit were added to complete the intact L4-L5-S1 unit. The

mechanical properties of the components added were assumed to be equal to those of the L4-L5 segment. The L5-S1 segment was calibrated in the intact condition since the step-wise reduction method had not been carried out for this segment. In this step, the ROM curves of the intact unit were compared with those obtained by Panjabi et al. [21] and Guan et al. [10], except for the axial rotation curve, which was not reported by Guan et al. [10]. During this stage, only the properties of the springs representing the contacting surfaces were modified to obtain a better adjustment of the experimental curves.

As the thickness of the facet cartilage is variable and the gap between the facets depends on the individual characteristics of the subject [28], we used five nonlinear springs on the facets to represent the contacting surfaces (Fig. 4). This strategy allowed a better control of the contact between the facets when the vertebral arches were activated. Each of these springs was able to modify a particular motion, e.g., for the control of the lateral flexion only the properties of the lateral-spring were changed. This procedure allowed the representation of the gap size between the facets by varying the force-displacement curves of the springs without modifying the geometry of the unit.

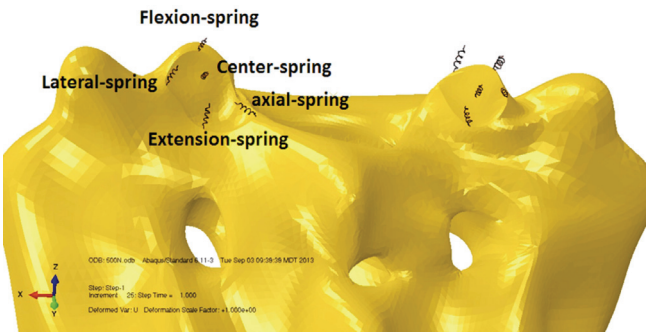

Fig. 4. Nonlinear springs representing the contact between the facet capsules

3. Results

We next present results of the model and compare them with reported experimental data. First, the model of the L4-L5 segment was able to provide a good approximation of the experimental data for all stages of the calibration protocol as shown for the reduced model with the annulus only (Fig. 5) and for the intact model (Fig. 6). In particular, the reduced model with the annulus only was able to clearly reproduce the neutral zone and the high degree of nonlinearity of the flexion, extension and axial rotation curves. A lower quality of adjustment was accomplished for lateral rotation. However, model predictions were near the extreme values obtained in the experimental tests. Good approximation of the experimental data was also accomplished with the intact model (Fig. 6).

a)

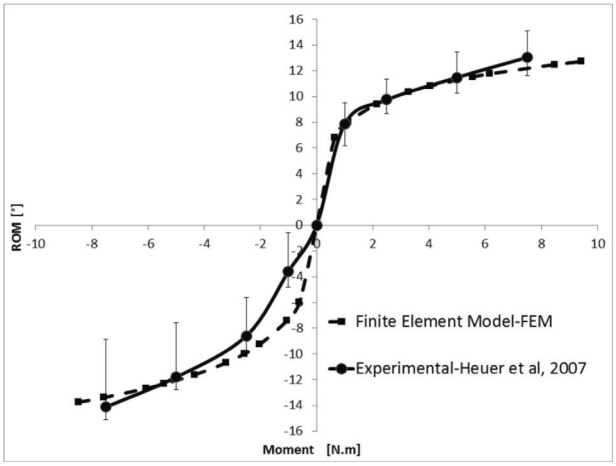

b)

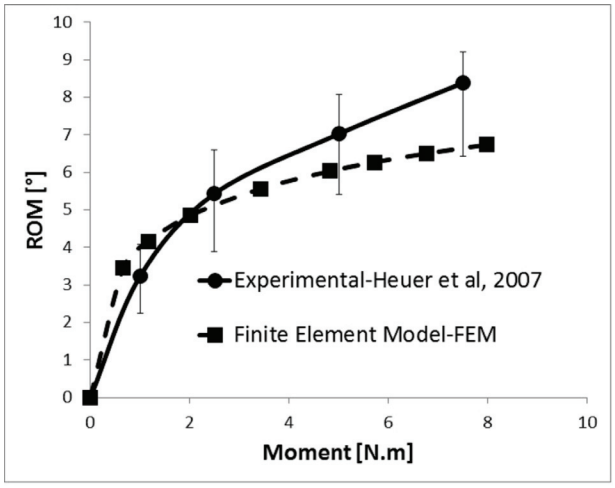

c)

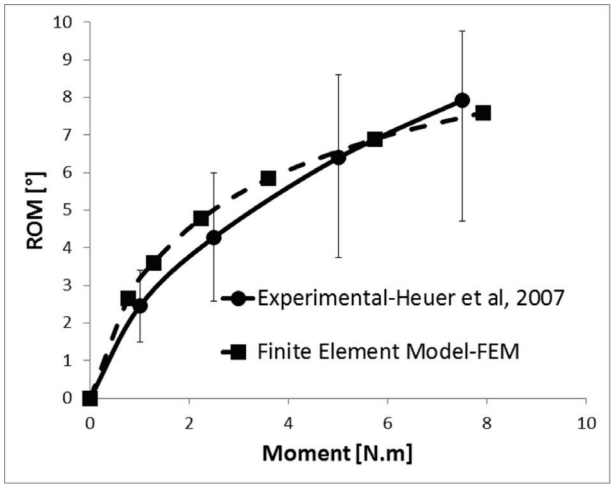

Fig. 5. Comparison of experimental and finite element ROM curves for the reduced L4-L5 segment (without ligaments, contact surfaces and nucleus) under: a) Flexion-Extension, b) lateral flexion, c) axial rotation

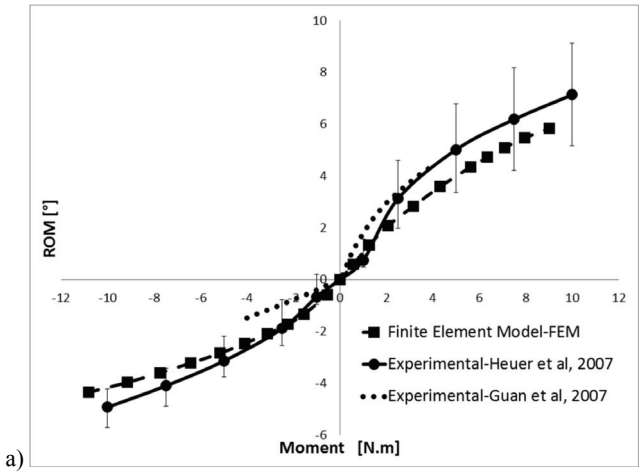

a)

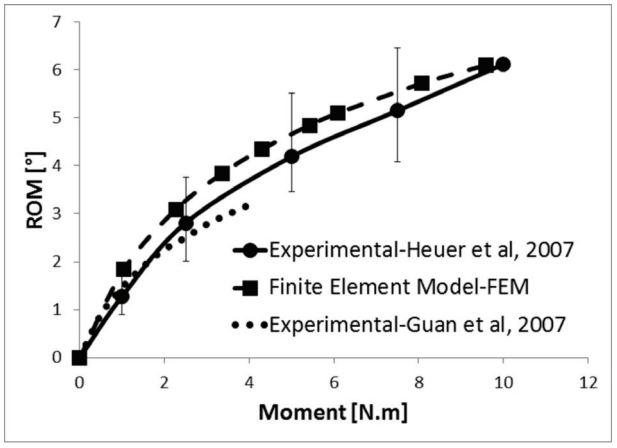

b)

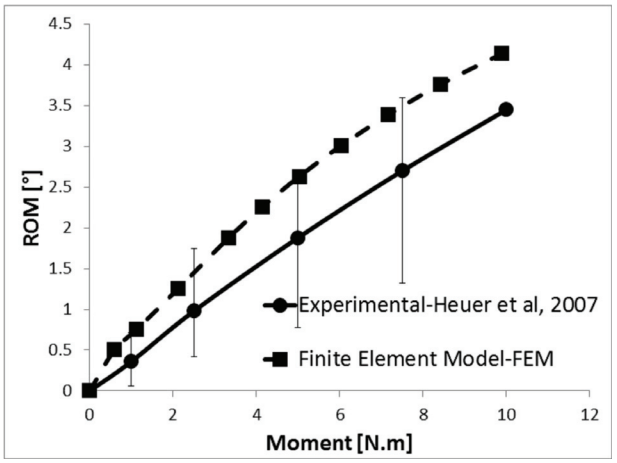

c)

Fig. 6. Comparison of experimental and finite element ROM curves for the intact L4-L5 segment under: (a) Flexion-Extension, (b) Lateral flexion, (c) Axial rotation

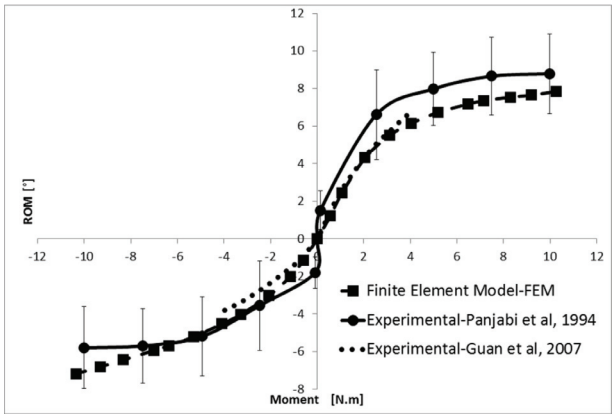

a)

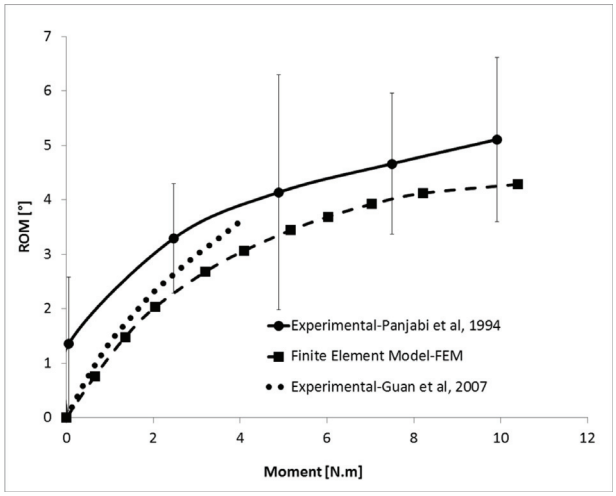

b)

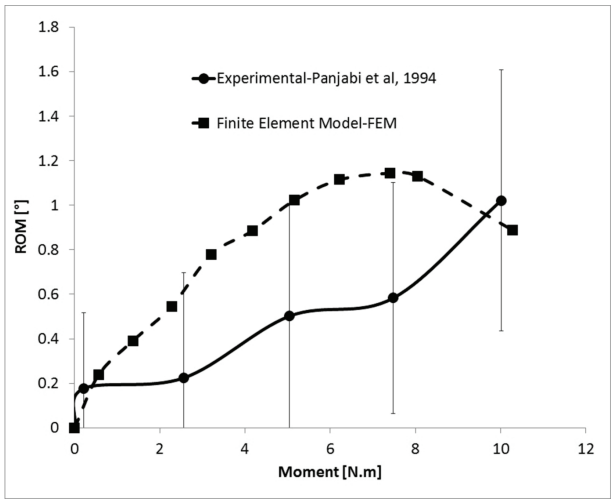

c)

Fig. 7. Comparison of experimental data and finite element model predictions for the L5-S1 segment with all the ligaments: (a) Flexion-Extension, (b) Lateral flexion, (c) Axial rotation

The ROM predictions for the intact L5-S1 model under flexion-extension and lateral rotations (Fig. 7) were closer to the experimental data reported by Guan et al. [10] and were within one standard deviation of the data reported by Panjabi et al. [21], with the exception of axial rotation.

The L4-L5 disc lateral bulging was higher under flexion for both the reduced and the intact segment (Fig. 8), which is consistent with experimental findings obtained for the L3-L4 segment by Heuer et al. [14].

Experimental bulging for the L3-L4 disc [14] was 12.8–30.6% lower than finite element predictions for the L4-L5 model under the action of 7.5 kN·m moments.

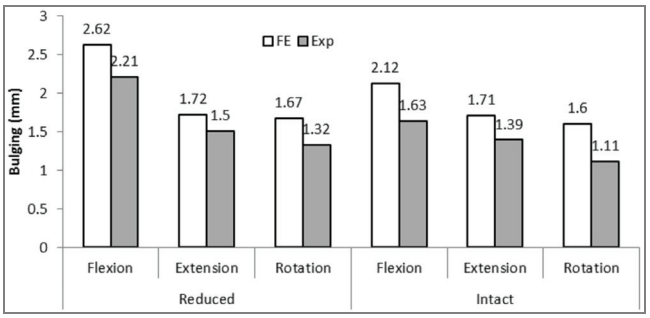

Fig. 8. Lateral bulging FE predictions for the L4-L5 disc and experimental (Exp) bulging for the L3-L4 disc under the action of moments equal to 7.5 kN-m [14]. The reduced model included only the vertebral bodies and the disc, consistent with experimental protocol

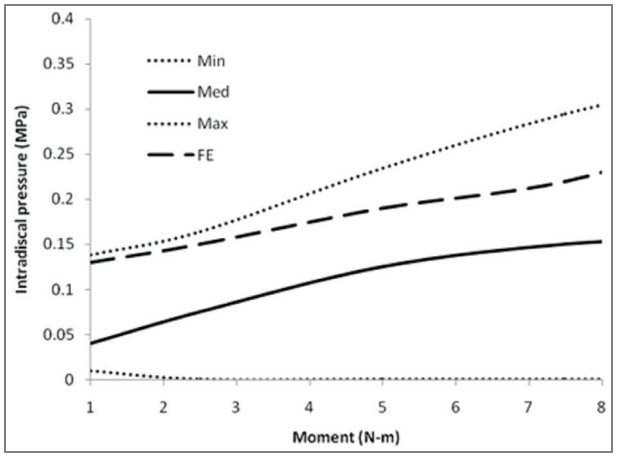

a)

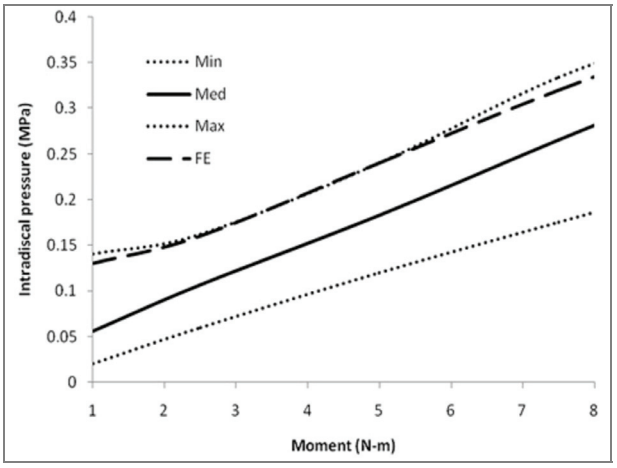

b)

Fig. 9. Comparison of the finite element intradiscal pressure (FE) and the median experimental values (Med) and the experimental range from minimum (Min) and maximum (Max) for extension. Experimental values by Heuer et al. [12]: (a) L4-L5 disc, (b) L5-S1 disc

Finite element predictions of the intradiscal pressure for the L4-L5 disc were within the experimental range obtained by Heuer et al. [12]. Under flexion-extension, finite element predictions were near the upper experimental values (Fig. 9). Moreover, under a compressive load of 2000 N, the finite element model predicted an approximately hydrostatic stress distribution in the nucleus depicted by the similarity between the horizontal and vertical stress components (Fig. 10) which were within one standard deviation of the experimental values of the nuclear pressure (1.74 ± 0.52 MPa) measured by Adams et al. [1].

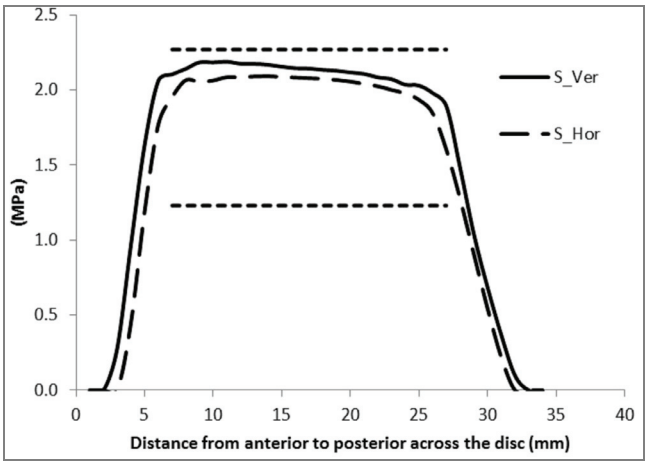

Fig. 10. Curves of the horizontal (S_Hor) and vertical (S_Ver) compressive stress components along the anteroposterior direction in the L4-L5 disc while the L4-L5-S1 was under a compressive force of 2000 N. The horizontal lines define the range within ± one standard deviation measured by Adams et al. [1]

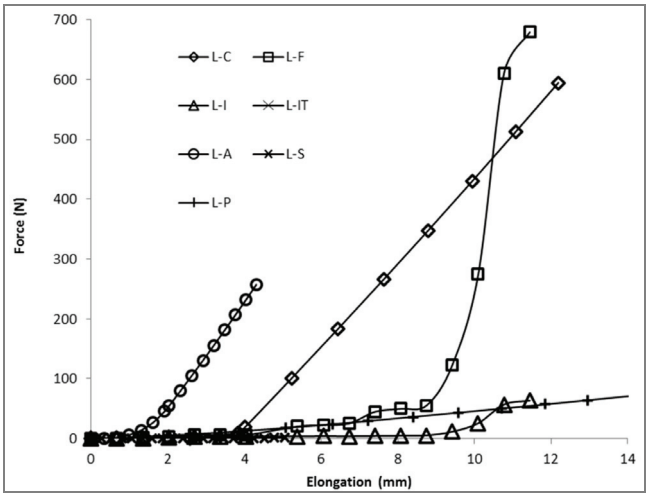

Fig. 11. Force-elongation curves in the calibrated model for the capsular ligament (L-C), the flavum (L-F), the interspinous (L-I), the intertransverse (L-IT), the anterior longitudinal (L-A), the supraspinous (L-S) and the posterior longitudinal (L-P)

Force-elongation curves of the ligaments (Fig. 11) depict a typical behavior characterized by an initial compliant zone followed by stiffening under strain. This behavior is consistent with the microstructure of the ligaments composed of crimped fibers that do not sustain load under low deformations and subsequently stiffen under higher strains, due to the increased alignment of the fibers in the direction of loading.

The constants c_1, c_2 and c_3 or the energy function of equation (1) were 0.015 MPa, –0.019 MPa and 0.041 MPa, respectively, while the constants a_1 and a_2 of Equation (2) describing the energy function of the fibers were in the ranges 0.65–1.20 MPa and 7.8–14.4, respectively (Table 1).

4. Discussion

A new model of the functional spine unit L4-L5-S1 was developed including a detailed representation of regional variations and anisotropy of the annulus as well as a realistic description of the nucleus geometry. The model may be used to provide and accurate description of mechanical parameters in the lumbar spine discs of workers performing risk-injury occupational activities such as lifting and carrying weights.

Since the model was oriented to analyze the stress distribution in the intervertebral discs, special attention was paid to consider details that may affect results. First, the model included a more realistic representation of the shape of the nucleus, which was created with its external perimeter following the boundary of the vertebral bodies. This form is different to the circular cross-sectional area assumed in other models [17]. In addition, this model took into account regional variations of material properties and the change of fiber orientation along the radial direction, which have been considered to be important factors affecting the biomechanics of the spine in previous L4-L5 models [22]. Compared to other models that include the L5-S1 disc [8], [11], the current model provides a more realistic representation of the vertebral bodies and a more precise modeling of the anisotropy of the annulus.

The parameters c_1, c_2, c_3 of the energy function of the annulus matrix equation (1) are equal to those reported by Ayturk et al. [2]. However, the parameters a_1 and a_2 of the energy function representing the fibers that were in the ranges 0.65–1.20 MPa and 7.8–14.4, respectively, are one order of magnitude different than the parameters reported by Ayturk et al. [2] for the L4-L5 segment, which are equal to 0.03 MPa and 120, respectively. It has to be noted that the parameter a_2 obtained in our study is more consistent with the direct measurements for human annulus tissue accomplished by Cortés et al. [5], who determined a range for a_2 equal to 5.64–8.78. Important differences with respect to the results by Ayturk et al. [2] may be due to both the regional variations of material properties and the change of fiber orientation with position that were taken into account in this study.

A detailed protocol using step-wise reduction experimental data for the L4-L5 segment [13] was followed for a proper validation of the model, which is an important step to guarantee that finite element predictions are realistic. Specifically, the step-wise calibration protocol allows an accurate assessment of the mechanical contribution of each component in the kinematic behavior of the unit. The curves of ROM vs moment displayed the main nonlinear features of the experimental curves at all stages of the step-wise reduction method. In addition, other parameters such as the intra-discal pressure and lateral bulging were close to the values reported in experimental studies.

FE predictions provided a good fitting of the experimental curves reported by Guan et al. [10] and Panjabi et al. [21] for the L5-S1 segment under flexion-extension and lateral bending, where model predictions were closer to experimental results by Guan et al. [10]. A higher degree of difference was obtained with respect to the form of the axial rotation experimental curve presented by Panjabi et al. [21], even though the terminal values at 10 N-m were similar (Fig. 7c). However, we have not found axial-rotation ROM curves reported for other FE models that include the L5-S1 disc [17] that may be used to compare with our FE predictions in order to understand the source of this difference.

The discrepancies of finite element model and experimental predictions for bulging may be attributed to the differences of cross-sectional area of the L4-L5 disc compared to experimental data for L3-L4 reported by Heuer et al. [14]. Another source of difference may be the loss of water during the step-wise experimental protocol, given the extensive time required to complete all tests. Due to this factor, the hydrated soft tissue became more compressible and consequently the lateral displacements were lower.

Some limitations are inherent to the developed model. First, vertebral bodies were considered to be rigid, which means that model predictions cannot be used to assess the stress distribution and the risk of

fracture in the bones. With respect to the mechanical predictions for the disc, a previous study [6] indicated that maximum stress and intradiscal pressure only changed a maximum of 2% when rigid bones were considered, compared to the predictions obtained with an accurate representation of the elasticity of the bones. The rigid-body assumption is also adopted in the recent model reported by Moramarco et al. [17]. Additionally, the rigid assumption for the bones implies important reductions on the time required to analyze the model. Another limitation is that the contacting surfaces were represented using nonlinear gap elements, meaning that the model is not capable of providing the stress distribution in the cartilage of the facets. Again, this representation of the contacting surfaces does not affect the stress distribution in the discs.

Acknowledgments

We acknowledge the support of COLCIENCIAS (contract 110651929063) to accomplish this study.

References

[1] ADAMS M.A., MCNALLY D.S., DOLAN P., *"stress" Distributions Inside Intervertebral Discs the Effects of Age and Degeneration*, J. Bone Joint. Surg. Br., 1996, 78-B, 965–972.

[2] AYTURK U.M., GARCIA J.J., PUTTLITZ C.M., *The Micromechanical Role of the Annulus Fibrosus Components Under Physiological Loading of the Lumbar Spine*, J. Biomech. Eng., 2010, 132, 061007–061007.

[3] BELLINI C.M., GALBUSERA F., RAIMONDI M.T., MINEO G.V., BRAYDA-BRUNO M., *Biomechanics of the lumbar spine after dynamic stabilization*, J. Spinal Disord. Tech., 2007, 20, 423–429.

[4] BOGDUK N., Clinical Anatomy of the Lumbar Spine & Sacrum, 1995.

[5] CORTES D.H., HAN W.M., SMITH L.J., ELLIOTT D.M., *Mechanical properties of the extra-fibrillar matrix of human annulus fibrosus are location and age dependent*, J. Orthop. Res., 2013, 31(11), 1725–1732.

[6] DIAZ C.A., GARCÍA J.J., PUTTLITZ C., *Influence of vertebra stiffness in the finite element analysis of the intervertebral disc*, ASME, Fajarado, Puerto Rico, USA, 2012, 2.

[7] EZQUERRO F., SIMÓN A., PRADO M., PÉREZ A., *Combination of finite element modeling and optimization for the study of lumbar spine biomechanics considering the 3D thorax–pelvis orientation*, Med. Eng. Phys., 2004, 26, 11–22.

[8] EZQUERRO F., VACAS F.G., POSTIGO S., PRADO M., SIMÓN A., *Calibration of the finite element model of a lumbar functional spinal unit using an optimization technique based on differential evolution*, Med. Eng. Phys., 2011, 33, 89–95.

[9] EZQUERRO JUANCO F., SIMÓN MATA A., MELLADO ARJONA E., VILLANUEVA PAREJA F., *Modelo de elementos finitos de la columna lumbar*, Biomecánica. 1999, VII, 46–52.

[10] GUAN Y., YOGANANDAN N., MOORE J., PINTAR F.A., ZHANG J., MAIMAN D.J. et al., *Moment–rotation responses of the human lumbosacral spinal column*, J. Biomech., 2007, 40, 1975–1980.

[11] GUAN Y., YOGANANDAN N., ZHANG J., PINTAR F.A., CUSICK J.F., WOLFLA C.E. et al., *Validation of a clinical finite element model of the human lumbosacral spine*, Med. Bio. Eng. Comput., 2006, 44, 633–641.

[12] HEUER F., SCHMIDT H., L. CLAES, WILKE H.-J., *Stepwise reduction of functional spinal structures increase vertebral translation and intradiscal pressure*, J. Biomech., 2007, 40, 795–803.

[13] HEUER F., SCHMIDT H., KLEZL Z., CLAES L., WILKE H.-J., *Stepwise reduction of functional spinal structures increase range of motion and change lordosis angle*, J. Biomech., 2007, 40, 271–280.

[14] HEUER F., SCHMIDT H., WILKE H.-J., *Stepwise reduction of functional spinal structures increase disc bulge and surface strains*, J. Biomech., 2008, 41, 1953–1960.

[15] JARAMILLO H.E., GARCÍA A., GÓMEZ L., ESCOBAR W., GARCÍA J.J., *Procedimiento para generar mallas de elementos finitos de la columna vertebral humana a partir de imágenes médicas*, Revista el Hombre y la Máquina, 2012, 40, 79–86.

[16] MEIJER G.J.M., HOMMINGA J., HEKMAN E.E.G., VELDHUIZEN A.G., VERKERKE G.J., *The effect of three-dimensional geometrical changes during adolescent growth on the biomechanics of a spinal motion segment*, J. Biomech., 2010, 43, 1590–1597.

[17] MORAMARCO V., PÉREZ DEL PALOMAR A., PAPPALETTERE C., DOBLARÉ M., *An accurate validation of a computational model of a human lumbosacral segment*, J. Biomech., 2010, 43, 334–342.

[18] NOAILLY J., WILKE H.-J., PLANELL J.A., LACROIX D., *How does the geometry affect the internal biomechanics of a lumbar spine bi-segment finite element model? Consequences on the validation process*, J. Biomech., 2007, 40, 2414–2425.

[19] NOAILLY J., *Model Developments for In Silico Studies of the Lumbar Spine Biomechanics*, Universidad Politecnica de Cataluña, Universidad Politecnica de Cataluña, España, 2009.

[20] O'CONNELL G.D., GUERIN H.L., ELLIOTT D.M., *Theoretical and Uniaxial Experimental Evaluation of Human Annulus Fibrosus Degeneration*, J. Biomech. Eng., 2009, 131, 111007.

[21] PANJABI M.M., OXLAND T.R., YAMAMOTO I., CRISCO J.J., *Mechanical behavior of the human lumbar and lumbosacral spine as shown by three-dimensional load-displacement curves*, J. Bone Joint. Surg., Series A, 1994, 76, 413–424.

[22] SCHMIDT H., HEUER F., SIMON U., KETTLER A., ROHLMANN A., CLAES L. et al., *Application of a new calibration method for a three-dimensional finite element model of a human lumbar annulus fibrosus*, Clin. Biomech., 2006, 21, 337–344.

[23] Seguro Social, Parámetros antropométricos de la población laboral Colombiana – 1995 Acopla 95, Seguro Social, Bogotá, 2002.

[24] TYNDYK M.A., BARRON V., MCHUGH P.E., O'MAHONEY D., *Generation of a finite element model of the thoracolumbar spine*, Acta Bioeng. Biomech., 2007, 9, 35–46.

[25] WANG J.L., PARNIANPOUR M., SHIRAZI-ADL A., ENGIN A.E., LI S., PATWARDHAN A., *Development and validation of a viscoelastic finite element model of an L2/L3 motion segment*, Theor. Appl. Fract. Mec., 1997, 28, 81–93.

[26] WEISSE B., AIYANGAR A.K., AFFOLTER C., GANDER R., TERRASI G.P., PLOEG H., *Determination of the translational and rotational stiffnesses of an L4-L5 functional spinal unit using a specimen-specific finite element model*, J. Mech. Behav. Biomed. Mater, 2012, 13, 45–61.

[27] WILKE H.-J., NEEF P., CAIMI M., HOOGLAND T., CLAES L.E., *New in vivo measurements of pressures in the intervertebral disc in daily life*, Spine, 1999, 24, 755–762.

[28] WOLDTVEDT D.J., WOMACK W., GADOMSKI B.C., SCHULDT D., PUTTLITZ C.M., *Finite element lumbar spine facet contact parameter predictions are affected by the cartilage thickness distribution and initial joint gap size*, J. Biomech. Eng., 2011, 133(6), 061009

[29] YOGANANDAN N., MYKLEBUST J.B., RAY G., PINTAR F., SANCES A., *A non-linear finite element model of a spinal segment*, Mathematical Modelling, 1987, 8, 617–622.